ERDC/ITL TN-21-1
September 2021

Thermal Camera Reliability Study: FLIR One Pro

By Quincy G. Alexander and Christo V. Lunderman

PURPOSE: The purpose of the effort described herein is to verify the reliability of the FLIR One Pro Gen 3 (FLIR One) unit through systematic experiments that compare the temperature perceived by the unit to the temperature measured by contact sensors on different materials through a range of temperatures.

BACKGROUND: The FLIR One unit was proposed for a larger study due to the relatively low cost (retail approximately $399),[1] thermal resolution, and the integrated visible spectrum camera. When connected to a mobile device, the FLIR One mobile app is used as the viewfinder and to control operation of the camera. The individual unit and the unit attached to a mobile device are shown in Figure 1. The thermal images captured using the FLIR One are taken at a resolution of 160 x 120 pixels in a "compressed image format," to minimize storage size and the complimentary software automatically upscales the images to 640 x 480 pixels (Alfonso 2019). The corresponding visible spectrum images are taken at resolution of 1440 x 1080 pixels. The FLIR One specifications state an object temperature range of -20°C to 400°C (-4°F to 752°F) and accuracy of ±3°C (5.4°F) or ±5%.[1]

Figure 1. FLIR One Pro device and connection to mobile device with app.

TEST SETUP: A test series was performed utilizing two specimens and two surface temperature measurement sensors to test the accuracy of the FLIR One.

- *Test Specimen 1* consisted of a steel plate clamped to a wooden base. A resistance temperature detector (RTD) sensor was microwelded to the plate to track the surface temperature through time at a discrete point. The RTD was produced by Hitec Products, Inc., part number TSW-00-D-GP-RTD; the sensor was calibrated by the manufacturer. Additionally, a strain gage was attached to the plate, but was not used for this effort.

[1] https://www.flir.com/products/flir-one-pro/

- *Test Specimen 2* consisted of a concrete cylinder with induced damage. A Campbell Scientific brand Surface-Mount Thermistor (model 110PV-L), with a 1-inch diameter contact disk used as the temperature measuring device, was clamped to the cylinder to measure the surface temperature.

The two instrumented test samples were placed inside an environmental chamber where the temperature cycled between highs of 49°C (120°F) degrees and lows of -23°C (-10°F). Within the test chamber, the cycles were set to run hot for 8 hr (05:00-13:00) and cold for 16 hr (13:00-05:00). An additional thermocouple sensor was placed in the chamber near the concrete specimens to measure the chamber temperature. There was a large variance in temperature along the height of the test chamber during the heating cycle, therefore, the chamber temperature measurement only applied to the area near the thermocouple. The test samples were placed in the chamber for 1 week to fully acclimate to the chamber and collect preliminary data from the attached sensors. Data was collected using a Campbell Scientific data logger, model CR-1000. A sample rate of 5 min was used for each of the three sensors.

The temperature perceived by a thermal camera can vary for items at the same temperature, unless the image is tuned based on the material types evaluated. Therefore, some parameters about the material must be known to get a true temperature value. The parameters relate to the idea that thermal radiation will either be reflected, absorbed, or transmitted away from the material, and these properties vary by material type and surface conditions.[1] The total radiation law, shown in Equation 1, defines this process, where, ρ is the reflectivity, ε is the emittance or emissivity of the object, and τ is the transmissivity.

$$\rho + \varepsilon + \tau = 1 \tag{1}$$

A few idealized cases include a black body ($\varepsilon = 1$) where thermal radiation striking the object is only absorbed and a white body ($\rho = 1$) where all thermal radiation is reflected. The third ideal is a 100% transparent object ($\tau = 1$) where all thermal radiation passes through the body without a reduction in value. Note that both ideal black and white bodies are thermally opaque ($\tau = 0$), i.e., thermal energy does not pass through the body. This condition introduces the concept of a grey body where τ is 0 and the radiation law is only a function of ρ and ε. In this scenario, there is only one independent variable, as it is possible to use the radiation law to obtain ρ from ε , and vis-a-versa.

Thermal emissions follows similar principles, and while a perfect grey body does not exist (especially one with the same emissivity over all temperatures), the concept is important for the science of thermography because the perfect grey body is a good basis for relating infrared radiation to an object's temperature. For a grey body, emissivity represents the ratio of the energy emitted by an object relative to the energy that would be emitted by a black body (Equation 2).

$$\varepsilon = \frac{W_{obj}}{W_{bb}} \tag{2}$$

[1] https://www.flir.com/products/flir-one-pro/

where

W_{obj} = Radiated Energy of a Normal Body
W_{bb} = Radiated Energy of a Black Body at the Same Temperature

Black electrical tape is thermally opaque with a known emissivity (ε) value of 0.95[1] at the temperature ranges of interest. Therefore, a piece of black electrical tape was placed on each specimen near the sensor location to represent an area of known emissivity. With emissivity known at the location of the black tape, the true temperature can be measured. The test setup is shown in Figure 2.

TEST RESULTS: The data logger recorded temperature at 5-minute intervals throughout the test period. Incrementally, thermal images were taken of an area on the front and back of the steel plate and the area of the concrete cylinder near the sensor location. Several thermal images were taken at each time interval. In post-processing, an emissivity value of 0.95 was applied to the thermal scenes, and apparent temperature was "measured" at target locations near the sensor. The measured thermal values for each time increment were averaged. A sample infrared image of the front of the steel plate (the side with the contact sensors) and the concrete sample is shown in Figure 3.

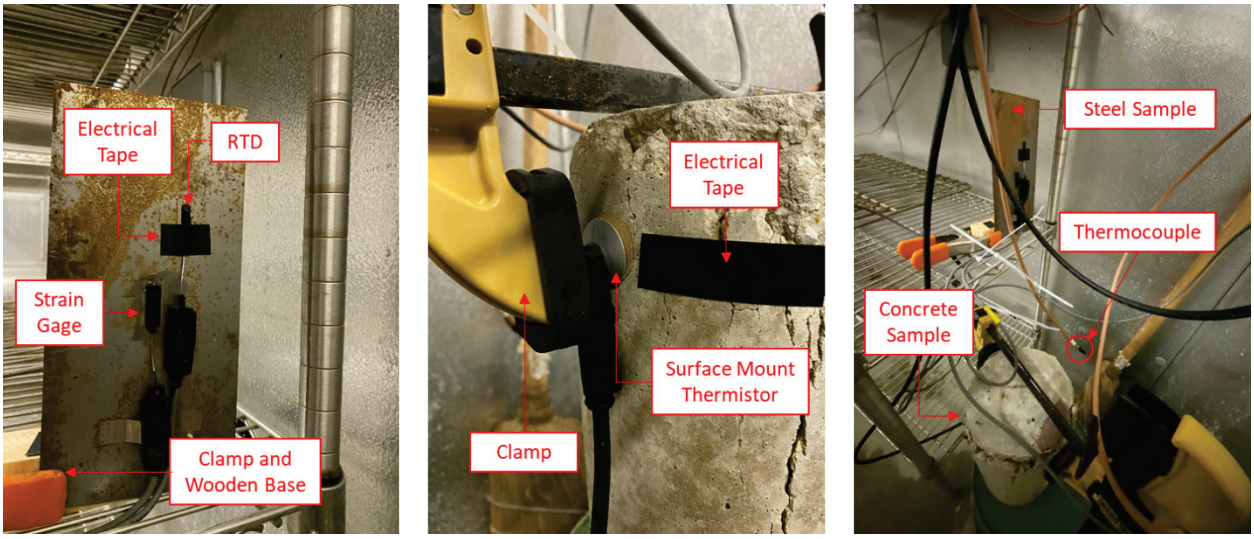

Figure 2. (a) Steel test specimen, (b) concrete test specimen, and (c) test setup in chamber.

Steel plate. The summary of results for this test series are provided in Table 1 and Figure 3. The thermal image temperature reading was measured on the electrical tape, near the contact sensor. The average temperature difference between the RTD measurement and the thermal image values for the steel plate was -0.32 °F. The object temperature for tests 16-18 was below the minimum specified range for the camera, though the camera still performed well in that range. All tests show a temperature difference less than or equal to the specified accuracy of 5.4 °F.

[1] FLIR, "Use Low-Cost Materials to Increase Target Emissivity," 05 November 2015. [Online]. Available: https://www.flir.com/discover/rd-science/use-low-cost-materials-to-increase-target-emissivity/. [Accessed 26 May 2020].

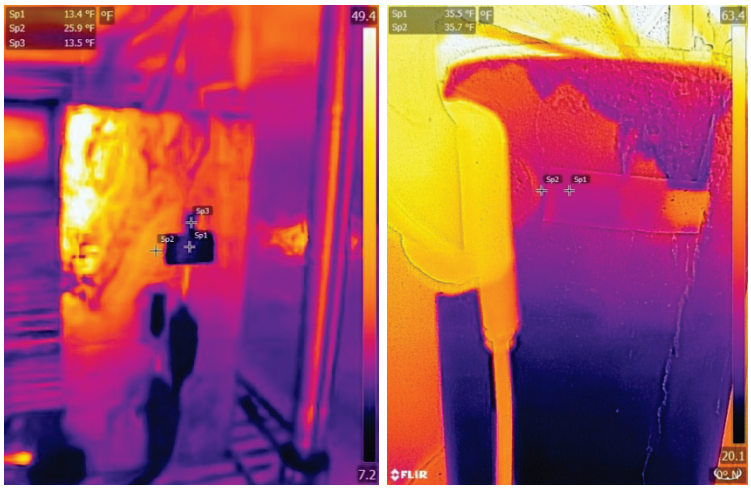

Figure 3. Thermal image from steel and concrete test sample.

Table 1. Steel plate comparison of RTD and thermal imaging temperature measurements.

Test	Time	RTD Recorded Temp, °F	Average Thermal Image Temp, °F	Temperature Difference, °F
1	5:20 AM	74.81	75.25	-0.44
2	5:30 AM	74.22	75.33	-1.11
3	6:00 AM	75.23	77.05	-1.82
4	6:30 AM	83.1	83.20	-0.10
5	7:00 AM	87.7	86.40	1.30
6	7:30 AM	85.8	91.12	-5.32
7	8:00 AM	93.1	93.03	0.07
8	8:30 AM	90.3	93.96	-3.66
9	10:30 AM	103.5	108.90	-5.40
10	11:00 AM	106.9	110.15	-3.25
11	11:30 AM	92.4	89.22	3.18
12	12:00 PM	53.16	52.47	0.69
13	1:45 PM	11.59	11.81	-0.22
14	2:05 PM	16.64	12.40	4.24
15	2:30 PM	1.176	0.01	1.16
16	3:00 PM	-7.453	-8.41	0.95
17	3:30 PM	-8.72	-7.03	-1.69
18	5:00 PM	-8.35	-11.60	3.25

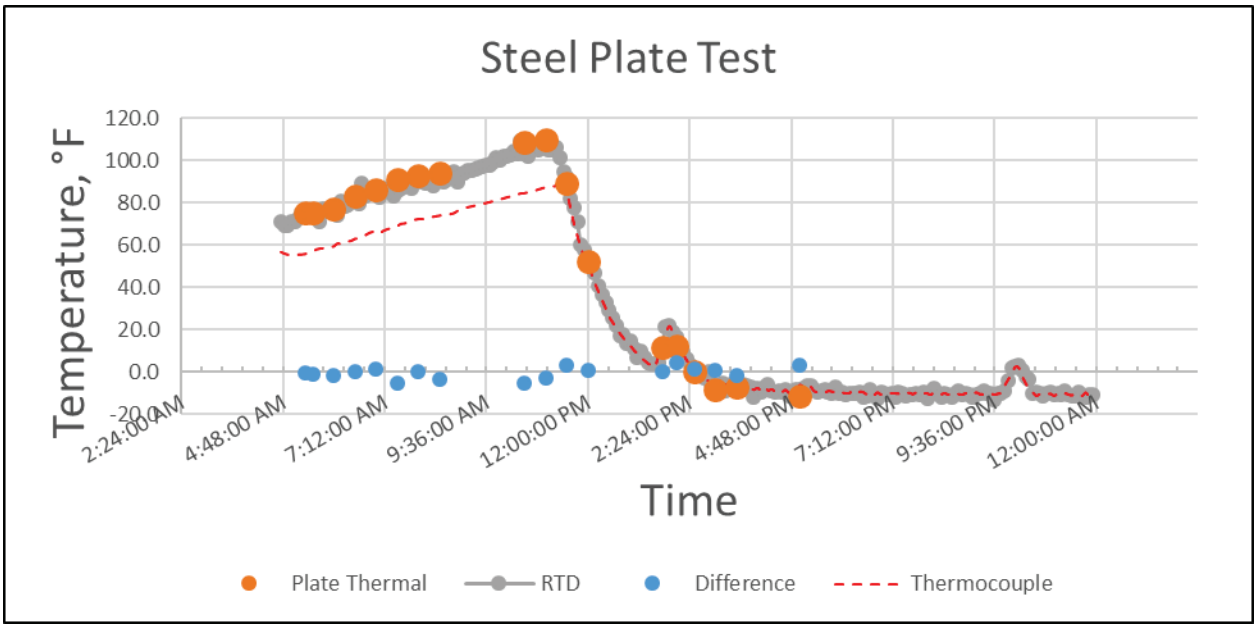

Figure 4. Temperature-time history comparison of RTD and thermal imaging temperature measurements.

As seen in Figure 4, during the heating period (5:00 am – 11:00am), the test sample was warmer than the ambient air temperature measured by the thermocouple but aligns very well during the cooling period. This is because the thermocouple was positioned lower than the steel plate test sample in the chamber, aligning with the position of the concrete sample (Figure 2(c)). When heating, there was a significant temperature gradient along the height of the chamber, with the warmest air (~130 °F) near the top and cooler air (~88 °F) near the bottom (Figure 5 (b)). During cooling, however, the temperature variation along the height was not significant, ranging from 20 °F to 28 °F (Figure 5 (c)). As such, the thermocouple and test sample align well during the cooling period (11:00 a.m. –12:00 a.m.).

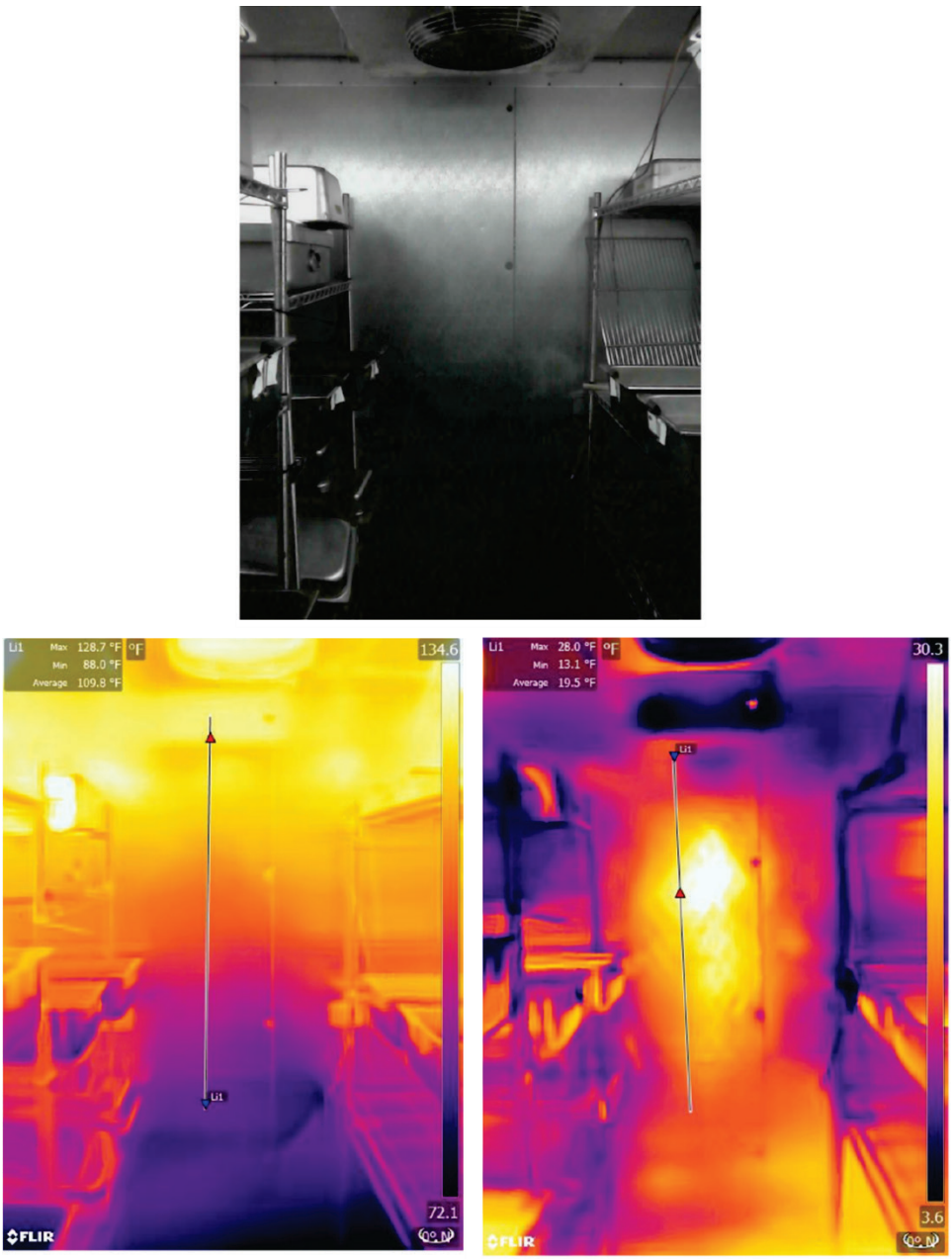

Figure 5. (a) Environmental chamber (b) thermal gradient during heating and (c) thermal gradient during cooling.

Concrete cylinder. The results for the concrete cylinder are provided in Table 2 and Figure 6. The average temperature difference between the surface-mount thermistor measurement and the thermal image values for the concrete cylinder was 3.3 °F. The object temperature for test 18 was below the minimum specified range for the camera, and the camera performed poorly in that range. All tests within the specified object temperature range showed a temperature difference less than or equal to the specified accuracy of 5.4 degrees, except Test 14, which showed a difference of 5.6 °F. During the time period of Test 14, there was a sudden rise and fall of the chamber temperature and the larger difference may simply be due to the approximation of time when the image was taken.

Because of the larger thermal mass of the concrete cylinder, Figure 6 shows there is a larger lag between the change in temperature relative to the thermocouple, as compared to the steel plate test. However, the high and low temperatures of the sample and the thermocouple correspond well.

Table 2. Concrete cylinder comparison of thermistor and thermal imaging temperature measurements.

Test	Time	RTD Recorded Temp, °F	Average Thermal Image Temp, °F	Temperature Difference, °F
1	5:20 AM	40.99	36.40	4.59
2	5:30 AM	43.15	39.45	3.70
3	6:00 AM	49.01	46.20	2.81
4	6:30 AM	54.23	50.94	3.29
5	7:00 AM	61.81	56.99	4.82
6	7:30 AM	66.24	64.70	1.54
7	8:00 AM	70.07	68.04	2.03
8	8:30 AM	72.43	68.33	4.10
9	10:30 AM	83	82.43	0.57
10	11:00 AM	85.8	82.66	3.14
11	11:30 AM	84.3	82.60	1.70
12	12:00 PM	69.8	66.92	2.88
13	1:45 PM	29.91	28.50	1.41
14	2:05 PM	29.78	24.18	5.60
15	2:30 PM	23.95	21.04	2.91
16	3:00 PM	17.45	13.83	3.62
17	3:30 PM	12.79	11.20	1.59
18	5:00 PM	2.87	-6.28	9.15

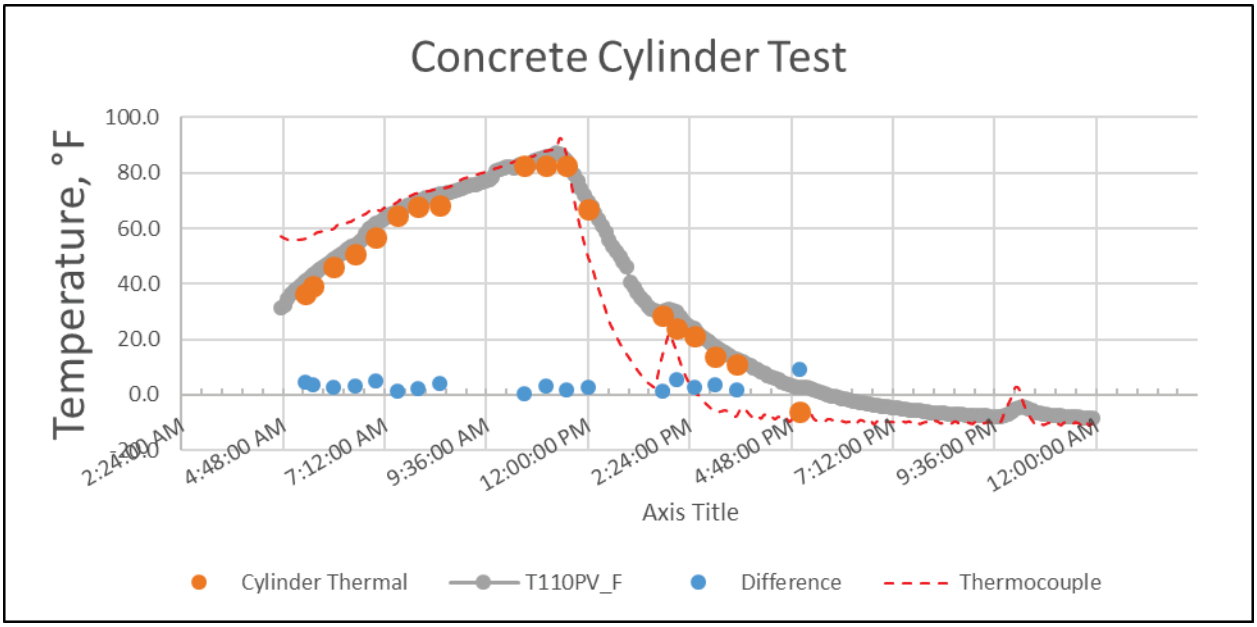

Figure 6. Temperature-time history comparison of thermistor and thermal imaging temperature measurement.

Emissivity. The infrared images were tuned to the known emissivity of the black tape (0.95), however, the appropriate value for the steel plate and the damaged concrete cylinder could be determined by adjusting the local emissivity value of a point on the material near the black tape, so the perceived temperatures match. Average emissivity values for different steel and concrete finishes are provided in Table 3.[1] For the concrete test sample, the temperature from a spot measurement taken near the black tape typically aligns with the temperature of the black tape, therefore, the assumed emissivity value of 0.95 can be assumed to be accurate. This is consistent with the published value for rough concrete.

Table 3. Published emissivity values for concrete and steel.

Material	Emissivity
Concrete	0.85
Concrete, Rough	0.94
Steel Oxidized	0.79
Steel Polished	0.07
Stainless Steel, weathered	0.85
Stainless Steel, polished	0.075
Stainless Steel, type 301	0.54 - 0.63
Steel Galvanized Old	0.88
Steel Galvanized New	0.23

For the steel test sample, the temperature from a spot measurement taken near the black tape was typically significantly different from the measured temperature on the black tape. The temperature varied from 5 °F -15 °F degrees at the high and low temperature extremes. This would imply that the emissivity of the steel plate was lower than 0.95. To better understand the appropriate emissivity value, the back of the plate was used for calibration. Similar to the primary test, an electrical tape target was placed on the back of the plate, as shown in Figure 7, and used to calibrate for emissivity. A nearby point was measured and the local parameters at the point were changed to a value where the two temperatures aligned. Using this approach, the emissivity value for the steel plate was determined to be approximately 0.82. This falls within the range of the published oxidized and weathered steel values, therefore it seems reasonable.

[1] e. Toolbox, "Emmissivity Coefficiients Materials," 2003. [Online]. Available: https://www.engineeringtoolbox.com/emissivity-coefficients-d_447.html. [Accessed 26 May 2020].

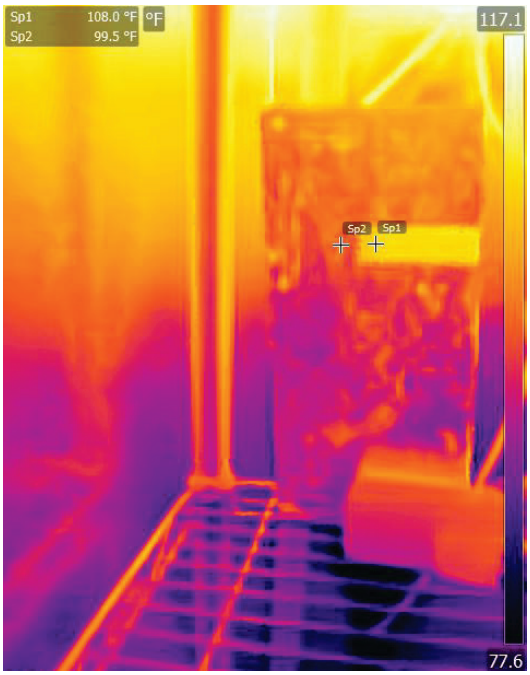

Figure 7. Thermal image of emissivity test setup for steel plate.

Curvature correction. A further study was performed to understand why the temperature difference between the contact sensor and thermal imaging was larger for the concrete tests than for the steel plate test. Cheng et al. (2012) concluded that the viewing angle of a curved surface can have a significant impact on the perceived temperature. The authors noted a good correlation when the view angle is 0 degrees (camera perpendicular), a noticeable reduction in the accuracy of perceived temperature occurring at viewing angles less than 60 degrees, and a significant reduction when the viewing angle exceeds 60 degrees. Due to the position of the concrete cylinder target area during the study described herein, most thermal images were taken with a view angle approximated to be between 20-60 degrees. This section seeks to further describe the impact the view angle may have on the results.

A metallic container, 4-inch in diameter by 6-inch tall was used to evaluate the impact of curvature on perceived infrared measurements. The container was filled with water to maintain a consistent temperature. Vertical strips of black electrical tape were added to identify the viewing angle of 0, -45, and 90 degrees. Additionally, a horizontal band of electrical tape was placed 1-1/2-inches, centered, from the bottom of the container. The FLIR Pro thermal camera was placed 4-1/2 inches from the container for the imaging. The thermal image was taken, and spot measurements were collected at the vertical tape locations and at intermediate targets centered between the vertical strips. The plan configuration is illustrated in Figure 8 and the interrogated image is shown in Figure 9.

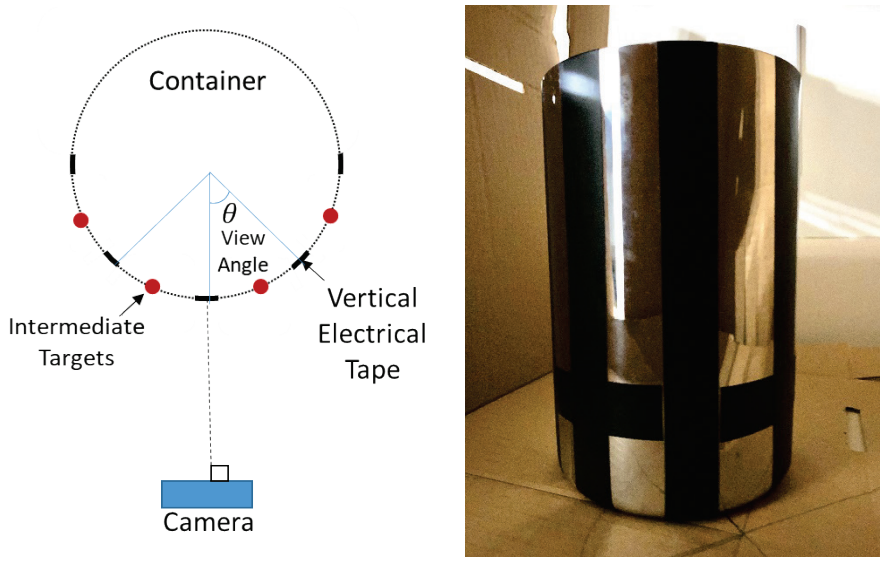

Figure 8. Test configuration and container with tape.

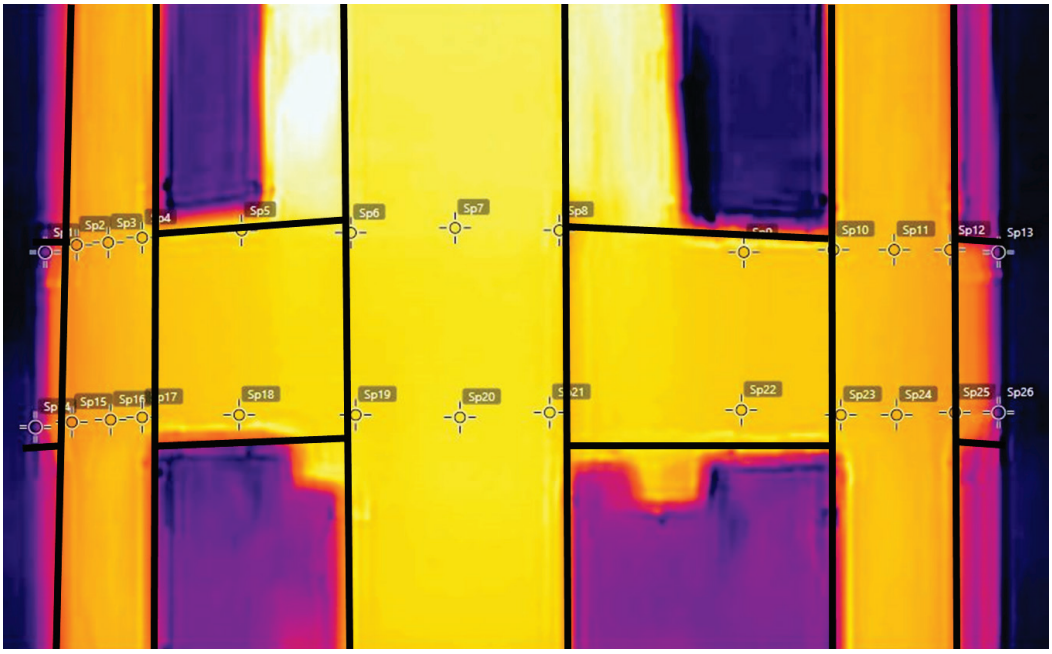

Figure 9. Thermal image with spot measurement locations.

The normalized equation described by Cheng et al. (2012) to capture the measurement error as a function of the view angle is provided in Equation 3. The apparent temperature measurements for each viewing angle, as determined from the thermal images, were applied to the equation, and the resulting errors are plotted by angle in Figure 10. The atmospheric temperature was determined to be 76 °F.

$$\Delta T = \frac{T_n - T(\theta)}{T_n - T_a} \quad (3)$$

where

ΔT = Normalized Error
T_n = Temperature at normal angle (θ=0)
$T(\theta)$ = Measured Temperature at Viewing Angle
T_a = Atmospheric Temperature

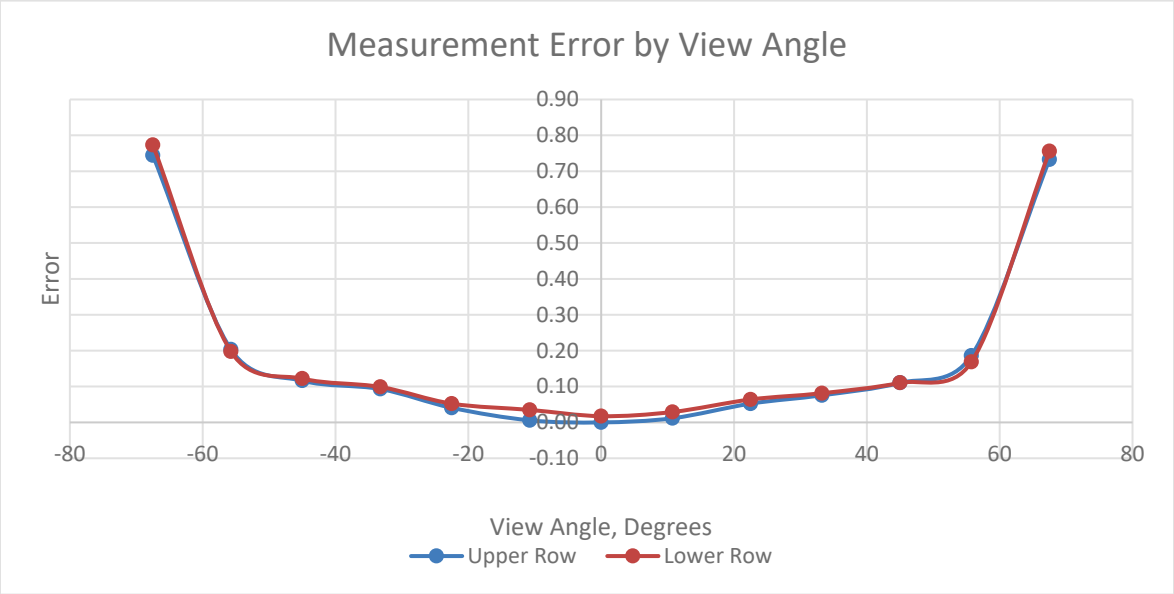

Figure 10. Measurement error by view angle.

The results indicate that small changes to the view angle will reduce the accuracy of the perceived temperature from thermal imaging, and the difference becomes significant at large angles. Due to the position of the concrete sample in the thermal chamber, the view angle was estimated to be in the 20-40-degree range. Per the study, this could cause the temperature to be underestimated by 2-3 °F. This is consistent with what is shown in Table 2, where the infrared measurement is typically approximately 3 °F less than the value measured by the contact thermistor.

SUMMARY: The Flir One Pro thermal camera is proposed for a study on an application of infrared thermography towards infrastructure inspection. Passive infrared thermography has shown potential for highlighting damage such as cracks and spalling, with proper consideration for diurnal effects (Alexander 2019). The thermal camera model was chosen due to its relatively low price point, good thermal resolution, and dual-lens (visible and thermal) imagery system. To verify the reliability of the camera, a test series was performed using a steel plate sample and a concrete cylinder sample, each with contact sensors to measure surface temperature. The samples were placed in an environmental chamber and subjected to a series of freeze/thaw cycles.

Through a single freeze-thaw cycle, thermal images were taken intermittently using the Flir One camera, and the results were compared to the temperatures measured by the contact sensors. The thermal camera performed within the specified tolerances during this test series when the object temperature was within the appropriate range. When the temperature fell below the lower

operating range, the unit's accuracy was reduced. The average error for the steel specimen was -0.32 °F and the average error for the concrete specimen was 3.3 °F, when the temperature was within the object operating range.

By comparing the temperature measured through the infrared images at the target of known emissivity to the bare test samples, it was determined that the concrete sample emissivity value was comparable to that for the electrical tape (0.95). The emissivity for the steel test sample was approximately 0.82. These values are reasonable when compared to the published literature for the two materials.

It was validated that for a cylindrical specimen, the view angle can significantly impact the perceived temperature measured using infrared. For this study, smaller view angles likely reduced the perceived temperature by 2-3 °F. This is consistent with the noted difference between the contact thermistor results and the thermal imagery results, which showed an average error of approximately 3 °F.

Based on the findings of this study, it was determined that the FLIR One Pro is a reliable unit when operating within the specified temperature, and accurate temperatures can be perceived when the scene is tuned based on the material and condition of the target structure.

REFERENCES

Alexander, Q. G., Hoskere, V., Spencer, B. F. Jr. and Smith, M. D. 2019. "Towards the Application of Image Based Monitoring of USACE Large Civil Infrastructure," *International Workshop for Structural Health Monitoring*, Palo Alto, CA.

Alfonso, D. 2019. "FLIR Tools-image resolution [Incident: 190409-000014]."

Cheng, T.-Y., D. Deng, and C. Herman. 2012. "CurvatureE Effect Quantification for In-Vivo IR Thermography." *International Mechanical Engineering Congress Expo*.